AIAA JOURNAL
Vol. 42, No. 6, June 2004

Oblique-Shock-Wave/Boundary-Layer Interaction Using Near-Wall Reynolds Stress Models

G. A. Gerolymos,* E. Sauret,† and I. Vallet‡
Université Pierre-et-Marie-Curie, 75252 Paris, France

A synthesis is presented of the predictive capability of a family of near-wall wall-normal free Reynolds stress models (which are completely independent of wall topology, i.e., of the distance from the wall and the normal-to-the-wall orientation) for oblique-shock-wave/turbulent-boundary-layer interactions. For the purpose of comparison, results are also presented using a standard low turbulence Reynolds number k–ε closure and a Reynolds stress model that uses geometric wall normals and wall distances. Studied shock-wave Mach numbers are in the range $M_{\mathrm{SW}} = 2.85$–2.9 and incoming boundary-layer-thickness Reynolds numbers are in the range $Re_{\delta_0} = 1$–2×10^6. Computations were carefully checked for grid convergence. Comparison with measurements shows satisfactory agreement, improving on results obtained using a k–ε model, and highlights the relative importance of redistribution and diffusion closures, indicating directions for future modeling work.

Nomenclature

$C_{f\infty}$	=	skin friction, $\bar{\tau}_w / \frac{1}{2}\bar{\rho}_\infty V_\infty^2$
c_p	=	heat capacity at constant pressure
h	=	enthalpy
k	=	turbulence kinetic energy, $\frac{1}{2}\widetilde{u_i'' u_i''}$
ℓ_T	=	turbulence length-scale, $k^{3/2}\varepsilon^{-1}$
M	=	Mach number
M_{SW}	=	Mach number upstream of the shock wave
P_k	=	turbulence kinetic energy production, $\frac{1}{2}P_{\ell\ell}$
Pr_T	=	turbulent Prandtl number
p	=	pressure
Re	=	Reynolds number
R_g	=	gas-constant, $\rho R_g T$
T	=	temperature
T_u	=	turbulence intensity, $\sqrt{(\frac{2}{3}k)}\tilde{V}^{-1}$
t	=	time
u_ℓ (u, v, w)	=	velocity components
V	=	velocity
x_ℓ (x, y, z)	=	Cartesian system of coordinates
α_c	=	ramp angle
γ	=	isentropic exponent
$\Delta\vartheta_{\mathrm{SW}}$	=	shock-wave turning angle
δ_{ij}	=	Kronecker symbol (components of the order-two identity tensor)
ε	=	turbulence kinetic energy dissipation rate
ε^*	=	turbulence kinetic energy modified dissipation-rate, $\varepsilon - 2\check{\nu}(\mathrm{grad}\sqrt{k})^2$
μ	=	dynamic viscosity
ν	=	kinematic viscosity
ρ	=	density
τ_{ij}	=	viscous stresses

Subscripts

e	=	conditions at the boundary-layer edge
i, j, k, ℓ	=	vector or tensor components along the corresponding direction or coordinate
T	=	turbulent
t	=	total thermodynamic quantities
w	=	wall
x, y, z	=	vector or tensor components along the corresponding coordinate
0	=	conditions at the beginning of the interaction
∞	=	conditions at infinity

Superscripts

$\tilde{}$	=	Favre average
$''$	=	Favre fluctuations
$\bar{}$	=	Reynolds average (ensemble average)
$\check{}$	=	function of averaged quantities that is neither a Favre average nor a Reynolds average[50]

Introduction

In numerous aerospace applications,[1,2] oblique-shock-wave/turbulent-boundary-layer interactions are important. Predictions of the interaction flowfields using Favre–Reynolds averaged methods with traditional turbulence models (zero-equation, one-equation, and two-equation Boussinesq closures or explicit algebraic Reynolds stress models) do not give satisfactory results, especially in the presence of large separation.[3–8] Note that, even when separation is small, the surface heat transfer coefficient, at high supersonic Mach numbers, can be unsatisfactorily predicted.[5] The use of more advanced realizable two-equation closures improves the overall behavior.[6,7] Rizzetta[7] obtained quite poor results using explicit algebraic Reynolds stress models (EARSMs) for $M_\infty \cong 3$ oblique-shock-wave/turbulent-boundary-layer interaction and concluded that the Speziale–Abid[9] realizable k–ε model gave the best overall results. Liou et al.[6] also obtained the best overall results using the realizable k–ε model of Shih et al.[10] Goldberg et al.[8] have studied $M_\infty \cong 8$ interactions and have highlighted the problems in correctly predicting surface heat transfer. Large-eddy simulation (LES) computations are a promising alternative, but high computing-time requirements limit, for the moment, this approach to relatively low Reynolds numbers (often two orders of magnitude below experimental conditions[11–14]).

Full Reynolds stress model (RSM) seven-equation closures have not yet been widely used in complex configurations, despite some early promising attempts. As early as 1980, Wilcox and Rubesin[15]

Received 2 May 2003; presented as Paper 2003-3466 at the 33rd Fluid Dynamics Conference, Orlando, FL, 23–26 June 2003; revision received 29 October 2003; accepted for publication 13 November 2003.

*Professor, Director, Laboratoire d'Energétique, Case 800, 4 place Jussieu; geg@ccr.jussieu.fr.
†Research Assistant, Laboratoire d'Energétique, Case 800, 4 place Jussieu; sauret@ccr.jussieu.fr.
‡Assistant Professor, Laboratoire d'Energétique, Case 800, 4 place Jussieu; vallet@ccr.jussieu.fr.

applied a near-wall Reynolds stress closure, using the ω_T scale-determining equation, to the computation of attached $M_\infty = 4$ boundary layers with adverse pressure gradient. Later, Wilcox[16] extended this model to a multiscale approach where one equation is solved for each Reynolds stress component of the energy-containing eddies spectral partition, together with the k–ω_T equations. This model was applied to the computation of an $M_\infty = M_{SW} = 2.85$, $\Delta\vartheta_{SW} = \alpha_c = 24$ deg compression corner (where $M_\infty = M_{SW}$ is the Mach number upstream of the shock wave), improving on the corresponding two-equation k–ω_T closure.[17] A further development of this model to a classical (not multiscale) RSM also gave satisfactory results.[18] Lee et al.[19] and Ladiende,[20] used compressible extensions of the Launder et al.[21] RSM (including dissipation–dilatation corrections, which are now known to be physically incorrect[22]) to study turbulent boundary-layer development on supersonic ($M_\infty = 2.87$) compression surfaces. Morrisson et al.[23] applied the near-wall RSM closure of Zhang et al.[24] to $M_\infty = 2.85$, $\alpha_c = 8$–20 deg compression-ramp flows, with quite satisfactory results. Chenault and Beran[25] and Chenault et al.[26] used this model to compute supersonic injection ($M_{inj} = 1.8$) into supersonic ($M_\infty = 3$) flows and obtained substantial improvements over k–ε results for highly three-dimensional flows. Sommer et al.[27] coupled the Zhang et al.[24] model with a k_θ–ε_θ model of thermal eddy diffusivity and applied the combination to many supersonic ($M_\infty = 2$–10) flat-plate boundary-layer flows. Zha and Knight[28] applied an RSM model (see Ref. 29) with the very simple rapid-pressure–strain closure $\phi_{ij2} = C_{p2}\bar{\rho}k(\partial\tilde{u}_i/\partial x_j + \partial\tilde{u}_j/\partial x_i)$, using wall functions, to the computation of three-dimensional shock-wave/boundary-layer interaction ($M_{SW} = 3.85$) due to a double-fin configuration and obtained a noticeable improvement in heat transfer prediction compared to the k–ε closure. Finally, Batten et al.[30] applied a modified cubic near-wall wall-normal free RSM (free from surface-topography parameters) to the computation of a three-dimensional $M_\infty = 2$ blunt-fin/flat-plate junction.

Supposedly high computing time requirements, numerical stability issues, and near-wall modeling are three frequently cited[7,9,31,32] issues that are offered as reasons for not using full seven-equation RSMs. Recent work on wall-normal free models[33–37] has rendered near-wall RSMs completely independent of wall topology. The careful numerical implementation of wall-normal free near-wall Reynolds stress closures renders such models both computationally efficient [local dual-time-stepping implicit time integration with specifically designed approximate Jacobians (see Ref. 38)] and robust (upwind discretization combined with the explicit application of realizability constraints[38]), for both steady and unsteady flows (efficient implementation of dual-time stepping[39]). These recent advances have made possible the application of wall-normal free near-wall RSMs to the computation of complex three-dimensional flows,[38–42] with quite promising results. The most important issue is that the availability of a robust computational method allows for systematic evaluation of full RSMs against benchmark configurations. Such systematic evaluation is of major importance because it will allow further optimization of RSMs for nonequilibrium highly inhomogeneous flows. Most available theories are for quasi-homogeneous quasi-equilibrium flow,[43–45] and even quite intricate inhomogeneous closures[46–48] have not yet been evaluated for a wide range of complex flows.

The purpose of the present paper is to present a synthesis of the predictive capability of a recently developed[34–36] family of near-wall wall-normal free RSMs for various oblique-shock-wave/turbulent-boundary-layer interactions. The two model variants considered in the present work differ mainly in the modeling of the rapid-pressure–strain terms and in the closure used for turbulent diffusion and offer insights to the relative influence of these processes for various flow regions.[35,36] Computations for each configuration are also run, for the purpose of comparison with baseline widely known closures, both using the Launder–Sharma k–ε closure[49] (which is also completely wall-normal-free) and the modified[50] near-wall RSM closure of Launder–Shima[51] (which uses geometric wall normals and distances from the wall). All computations were carefully checked for grid convergence using progressively finer grids. Computational predictions are compared with experimental measurements for three nominally two-dimensional configurations. The performance of the various models is carefully assessed, and recommendations for future modeling work are given.

Flow Model and Numerics

Flow Model

The flow is modeled using the Favre–Reynolds averaged Navier–Stokes equations. The working medium thermodynamics are approximated by a thermodynamically and calorically perfect gas ($\bar{p} = \bar{\rho}R_g\tilde{T}$ and $c_p = \gamma R_g/[\gamma - 1]$). All computations were run for air, $R_g = 287.04$ m^2 s^{-2} K^{-1} and $\gamma = 1.4$, and used a Sutherland law dependence for viscosity and a corrected Sutherland law for heat conductivity (see Ref. 34). The exact transport equations for the Favre–Reynolds averaged Reynolds stresses can be written symbolically:

$$C_{ij} = d_{ij} + P_{ij} + \phi_{ij} - \bar{\rho}\varepsilon_{ij} + K_{ij} + \tfrac{2}{3}\phi_p\delta_{ij} \tag{1}$$

where $\phi_{ij} = \overline{p'[\partial u_i''/\partial x_j + \partial u_j''/\partial x_i - 2/3(\partial u_k''/\partial x_k)\delta_{ij}]}$ is the pressure–strain redistribution, $d_{ij} = \partial(-\bar{\rho}\widetilde{u_i''u_j''u_\ell''} - \overline{p'u_j''}\delta_{i\ell} - \overline{p'u_i''}\delta_{j\ell} + \overline{u_i''\tau_{j\ell}'} + \overline{u_j''\tau_{i\ell}'})/\partial x_\ell$ is the diffusion due to turbulent transport (due to triple-velocity correlations, pressure fluctuations, and molecular viscosity), $P_{ij} = (-\bar{\rho}\widetilde{u_i''u_\ell''}\partial\tilde{u}_j/\partial x_\ell - \bar{\rho}\widetilde{u_j''u_\ell''}\partial\tilde{u}_i/\partial x_\ell)$ is the production due to the interaction with the mean flow gradients, $\phi_p = \overline{p'\partial u_k''/\partial x_k}$ is the pressure–dilatation correlation and $K_{ij} = (-\overline{u_i''}\partial\bar{p}/\partial x_j - \overline{u_j''}\partial\bar{p}/\partial x_i + \overline{u_i''}\partial\bar{\tau}_{j\ell}/\partial x_\ell + \overline{u_j''}\partial\bar{\tau}_{i\ell}/\partial x_\ell)$ are direct compressibility effects (density-fluctuation effects associated with $u_i'' \equiv \bar{u}_i - \tilde{u}_i = -\rho' u_i''/\bar{\rho}$). Convection C_{ij} and production P_{ij} are exact terms, whereas all of the other terms require modeling. In all of the models used in the present work, direct compressibility effects and pressure–dilatation were neglected:

$$K_{ij} \cong 0, \qquad \overline{u_i''} \cong 0, \qquad \phi_p \cong 0 \tag{2}$$

It is generally accepted[52] that these terms do not have a major influence in wall-bounded flows, and recent work by Pantano and Sarkar[22] indicates that the well-known free shear flow major compressibility effect might be due to compressibility damping of ϕ_{ij}.

For all of the models studied in the present work, the turbulence length scale determining equation is an equation for the modified dissipation rate ε^*:

$$\frac{\partial\bar{\rho}\varepsilon^*}{\partial t} + \frac{\partial}{\partial x_\ell}\left(\tilde{u_\ell}\bar{\rho}\varepsilon^*\right) - \frac{\partial}{\partial x_\ell}\left[\left(\breve{\mu}\delta_{k\ell} + C_\varepsilon\frac{k}{\varepsilon^*}\bar{\rho}\widetilde{u_k''u_\ell''}\right)\frac{\partial\varepsilon^*}{\partial x_k}\right]$$
$$= C_{\varepsilon 1}P_k\frac{\varepsilon^*}{k} - C_{\varepsilon 2}\bar{\rho}\frac{\varepsilon^{*2}}{k} + \frac{2\breve{\mu}\mu_T}{\bar{\rho}}(\nabla^2\tilde{\boldsymbol{V}})^2 \tag{3}$$

$$C_\varepsilon = 0.18, \qquad C_{\varepsilon 1} = 1.44, \qquad C_{\varepsilon 2} = 1.92\left(1 - 0.3e^{-Re_T^{*2}}\right)$$

$$\mu_T = C_\mu\breve{\mu}Re_T^*, \qquad C_\mu = 0.09\exp\left[-\frac{3.4}{\left(1 + 0.02Re_T^*\right)^2}\right]$$

$$Re_T^* = k^2(\breve{\nu}\varepsilon^*)^{-1}$$

where the Launder–Sharma[49] coefficients were used. The flow model consists of the five mean flow equations (continuity, momentum, and energy) together with Eqs. (1) and (3). Full details of the flow model are given by Gerolymos and Vallet.[34]

Turbulence Closures

For all of the computations presented in the present work, the turbulent heat flux was modeled by a simple gradient closure:

$$\bar{\rho}\widetilde{h''u_i''} = -\frac{\mu_T c_p}{Pr_T}\frac{\partial\tilde{T}}{\partial x_i}, \qquad Pr_T = 0.9 \tag{4}$$

This is a baseline closure and should be improved by using transport equation closures for the heat fluxes.[27] The following four turbulence closures were used for the Reynolds stresses.

Launder–Sharma[49] *k–ε*

The k–ε low-turbulence Reynolds number closure of Launder–Sharma[49] was used as a baseline two-equation model prediction, whose validity (and drawbacks) are well known. The detailed flow model and k–ε transport equations used are described in detail by Gerolymos and Vallet.[53] In the implementation used, the production of turbulence kinetic energy k is limited to twice the dissipation rate $P_k = \min(P_k, 2\bar{\rho}\varepsilon^*)$. Improved limitations could be used, following the approach of Durbin,[54] which is based on applying Schumann's realizability[55] constraints on the Boussinesq closure, but this was not attempted in the present study. (These limitations are inherently applied in realizable k–ε closures.[9,10])

Launder–Shima–Sharma RSM

The Launder–Shima–Sharma (LSS) closure is based on the Launder–Shima[51] seven-equation Reynolds stress closure that uses geometric wall normals, but where the Launder–Sharma[49] ε^* equation for the modified dissipation rate was used. This combination was introduced by Gerolymos and Vallet[50] and Vallet and Gerolymos[56] because the original ε equation of Launder–Shima exhibited severe relaminarization problems in accelerating supersonic flows, and more important, the Dirichlet boundary condition $\varepsilon^* = 0$ on a solid wall enhances the computational stability of the model. This choice of using ε^* has been adopted by other researchers addressing shock-wave/boundary-layer interaction flows.[30] The LSS closure uses the geometric distance from the wall and the geometric normal to the wall direction in the echo terms present in the redistribution closure. The detailed flow model and RSM closure with geometric wall normals are given by Gerolymos and Vallet.[50]

Gerolymos–Vallet[34] *RSM*

The Gerolymos–Vallet[34] (GV) RSM is fully wall-normal free, that is, independent of any geometric wall-topography-related parameter. This closure has been designed by introducing a unit vector pointing in the direction of inhomogeneity of the turbulent field, which replaces geometric wall normals in the echo terms appearing in the redistribution model[34] and a separate indicator for the magnitude of these echo (inhomogeneity) terms. This idea is an extension of previous work by Craft and Launder,[46] Craft,[47] and Craft et al.[57] who were the first introduce analogous models, but without separating the magnitude and direction of inhomogeneity indicators. In a recent work, various proposals for the inhomogeneity direction were reviewed[35] and the relation[34]

$$\boldsymbol{e}_I = e_{I_i}\boldsymbol{e}_i = \operatorname{grad}\left\{\frac{\ell_T[1-\exp(-Re_T/30)]}{1+2\sqrt{A_2}+2A^{16}}\right\}\Bigg/\left\|\operatorname{grad}\left\{\frac{\ell_T[1-\exp(-Re_T/30)]}{1+2\sqrt{A_2}+2A^{16}}\right\}\right\| \tag{5}$$

is proposed, where $A_2 = a_{ik}a_{ki}$ is the second invariant, $A_3 = a_{ik}a_{kj}a_{ji}$ is the third invariant of the anisotropy tensor $a_{ij} = \widetilde{u_i''u_j''}/k - \frac{2}{3}\delta_{ij}$, and $A = 1 - \frac{9}{8}(A_2 - A_3)$ is the flatness parameter introduced by Lumley.[44] This relation can be used in any existing RSM to replace the geometric unit normals. On the other hand, the model did not follow the complex cubic pressure–strain relations suggested by Craft and Launder,[46] but used instead the quasi-linear approach,[48] which requires the optimization of a reduced number of coefficients, introduces nonlinearity by making the model coefficients dependent on the Reynolds stress anisotropy-tensor invariants A_2, A_3, and their combination A (Ref. 44), and is much easier to implement numerically. The model for pressure–strain and dissipation terms reads

$$\begin{aligned}\phi_{ij} - \bar{\rho}\varepsilon_{ij} &= \left[\phi_{ij} - \bar{\rho}(\varepsilon_{ij} - \tfrac{2}{3}\delta_{ij}\varepsilon)\right] - \tfrac{2}{3}\delta_{ij}\bar{\rho}\varepsilon\\ &= \phi^H_{ij1} + \phi^H_{ij2} + \phi^I_{ij1} + \phi^I_{ij2} - \tfrac{2}{3}\delta_{ij}\bar{\rho}\varepsilon\\ &\cong -C_1^H\bar{\rho}\varepsilon a_{ij} - C_2^H\left(P_{ij} - \tfrac{1}{3}\delta_{ij}P_{\ell\ell}\right)\\ &\quad + C_1^I(\varepsilon/k)\left[\bar{\rho}\widetilde{u_k''u_m''}e_{I_k}e_{I_m}\delta_{ij} - \tfrac{3}{2}\bar{\rho}\widetilde{u_k''u_i''}e_{I_k}e_{I_j} - \tfrac{3}{2}\bar{\rho}\widetilde{u_k''u_j''}e_{I_k}e_{I_i}\right]\\ &\quad + C_2^I\left[\phi^H_{km2}e_{I_k}e_{I_m}\delta_{ij} - \tfrac{3}{2}\phi^H_{ik2}e_{I_k}e_{I_j} - \tfrac{3}{2}\phi^H_{jk2}e_{I_k}e_{I_i}\right] - \tfrac{2}{3}\delta_{ij}\bar{\rho}\varepsilon\end{aligned} \tag{6}$$

Another particularity of this model is the form of the functional dependence of the rapid pressure–strain coefficient C_2^H on the flatness parameter A [Eq. (9)]. The choice was motivated by the observation that in the regions of wake-type flows (separated flow regions, wake zone of the turbulent boundary layer) the parameter A is large (approaches unity because $A \in [0, 1]$) and the changes in value of C_2^H can enhance both the ability of the model to separate[34,40] as well as improve the prediction of three-dimensional secondary flows.[35,36] In summary,

$$d_{ij} = \frac{\partial}{\partial x_\ell}\left[\breve{\mu}\delta_{k\ell}\frac{\partial\widetilde{u_i''u_j''}}{\partial x_k} + C_s\frac{k}{\varepsilon}\left(\widetilde{u_i''u_k''}\frac{\partial\widetilde{u_j''u_\ell''}}{\partial x_k} + \widetilde{u_j''u_k''}\frac{\partial\widetilde{u_\ell''u_i''}}{\partial x_k} + \widetilde{u_\ell''u_k''}\frac{\partial\widetilde{u_i''u_j''}}{\partial x_k}\right)\right], \qquad C_s = 0.11 \tag{7}$$

$$C_1^H = 1 + 2.58AA_2^{\frac{1}{4}}\left\{1 - \exp\left[-\left(\frac{Re_T}{150}\right)^2\right]\right\} \tag{8}$$

$$C_2^H = \min[1, 0.75 + 1.3\max(0, A - 0.55)] \times A^{[\max(0.25, 0.5 - 1.3\max[0, A - 0.55])]}\left[1 - \max\left(0, 1 - \frac{Re_T}{50}\right)\right] \tag{9}$$

$$C_1^I = 0.83\left[1 - \frac{2}{3}\left(C_1^H - 1\right)\right]\left\|\operatorname{grad}\left\{\frac{\ell_T[1-\exp(-Re_T/30)]}{1+2A_2^{0.8}}\right\}\right\|$$

$$C_2^I = \max\left(\frac{2}{3} - \frac{1}{6C_2^H}, 0\right)\left\|\operatorname{grad}\left\{\frac{\ell_T[1-\exp(-Re_T/30)]}{1+1.8A_2^{\max(0.6, A)}}\right\}\right\| \tag{10}$$

Wall-Normal Free LSS RSM

The preceding model can be easily applied to the computation of complex three-dimensional flowfields because it combines ease of implementation (wall-normal free) and robustness. Application to a number of complex flows,[34–36,38–42] both two and three dimensional, including aircraft engine turbomachinery, has shown that it slightly overestimates separation, contrary to the LSS RSM with geometric normals. To study the relative importance of three modeling parameters: 1) redistribution coefficient C_2^H, 2) turbulent diffusion, and 3) the importance of using geometric normals or not, a wall-normal free (WNF) version of the LSS RSM was developed by Gerolymos et al.[35] (Note that LSS uses the Daly–Harlow[58] model and GV[34] uses the Hanjalić–Launder[59] model for the turbulent diffusion term.) This model retains the $C_2^H(A)$ of LSS RSM and the Daly–Harlow turbulent diffusion model, but replaces geometric normals with the inhomogeneity-direction indicator $\boldsymbol{e}_I$ [Eq. (5)]. The functions C_1^I and C_2^I were then optimized to get the correct plane-channel flow mean velocity and Reynolds stress profiles (see Ref. 35). The model can be summarized as

$$d_{ij} = \frac{\partial}{\partial x_\ell}\left[\left(\breve{\mu}\delta_{k\ell} + C_s\frac{k}{\varepsilon}\bar{\rho}\widetilde{u_k''u_\ell''}\right)\frac{\partial\widetilde{u_i''u_j''}}{\partial x_k}\right], \qquad C_s = 0.22 \tag{11}$$

$$C_1^H = 1 + 2.58AA_2^{\frac{1}{4}}\left\{1 - \exp\left[-\left(\frac{Re_T}{150}\right)^2\right]\right\}, \qquad C_2^H = 0.75\sqrt{A} \tag{12}$$

$$C_1^I = 0.90\left[1 - \frac{2}{3}\left(C_1^H - 1\right)\right]\left\|\operatorname{grad}\left\{\frac{\ell_T[1-\exp(-Re_T/30)]}{1+1.8A_2^{0.8}}\right\}\right\|$$

$$C_2^I = \max\left[\frac{2}{3} - \frac{1}{6C_2^H}, 0\right]\left\|\operatorname{grad}\left\{\frac{\ell_T[1-\exp(-Re_T/30)]}{1+1.8A_2^{\max(0.6, A)}}\right\}\right\| \tag{13}$$

Numerical Methods and Computational Grids

The computational algorithm[38] used in the present work discretizes the mean flow and Reynolds stress transport equations on a structured grid, using an $\mathcal{O}(\Delta x^3)$ upwind-biased MUSCL scheme, with van Leer flux-vector splitting, for the convective terms, and a standard centered $\mathcal{O}(\Delta x^2)$ scheme for the gradients appearing in the diffusive and the source terms. Time integration is implicit, and uses a local-dual-time stepping[38] approach (dual-time stepping with local time steps both for the time advancement and the subiterations). The number of subiterations performed at each iteration is based on a dynamic error-reduction criterion. Robust integration of the Reynolds stresses is achieved through the use of explicit realizability constraints[38] combined with the upwind space discretization. Computational efficiency is achieved through the particular choice of the approximate Jacobians used in the implicit phase of the method (see Ref. 38), resulting in only 26% overhead per iteration for the seven-equation RSM computations compared to two-equation computations. Dual-time stepping contributes in subiteratively correcting errors introduced by the approximate Jacobians or the approximate factorization. The numerical methodology[38] and its extension to unsteady flows[39] have been applied to the computation of various complex flows, and the RSM implementation has proven to be particularly robust.[34–36,38–42] The computational grids used were uniform in the streamwise direction. For the incident shock-wave case, one part of the grid was stretched geometrically near the wall, and the upper part of the grid was uniform. If N_j is the number of the grid points in the transverse direction, $N_{j_s} \leq N_j$ points are stretched geometrically with ratio r_j, whereas the remaining points are uniformly distributed. For the ramp test case, the same procedure applies for each half of the domain (between the upper/lower-wall and the centerline), so that for each half the same distribution applies with $(N_j/2+1)$ instead of N_j points. Furthermore, for all of the compression-ramp computations presented, stretching extended to the centerline ($N_{j_s} = N_j/2+1$). The flowfield is initialized by creating an inviscid flowfield consistent with the boundary conditions, to which are fitted boundary-layer profiles and external flow turbulence (Fig. 1), using the procedure described in Ref. 60.

Note that for the ramp test case the opposite wind-tunnel wall boundary layer was computed, whereas for the incident-oblique-shock cases, a subsonic inflow condition was used at the upper boundary, to avoid simulating the shock-generator configuration (Fig. 1).

Comparison with Experiments

Configurations Studied

The various turbulence closures were assessed by comparison with available experimental data for two configurations: 1) an incident oblique-shock-wave/turbulent-boundary-layer interaction, $M_{\mathrm{SW}} = 2.9$, $\Delta\vartheta_{\mathrm{SW}} = 13$ deg, and $Re_{\theta_0} = 4.7 \times 10^4$, studied experimentally by Reda and Murphy,[61] Murthy and Rose,[62] and Modaress and Johnson[63] and 2) compression-ramp configurations, $M_{\mathrm{SW}} = 2.85$, $\alpha_c = \Delta\vartheta_{\mathrm{SW}} = 20$–$24$ deg, and $Re_{\theta_0} = 8 \times 10^4$ studied experimentally by Settles et al.,[64] Horstman et al.,[65] Dolling and Murphy,[66] and Settles and Dodson.[67]

All of the computations were run by applying the experimental inflow conditions (Table 1). In Table 1, $M_\infty = M_{\mathrm{SW}}$ is the shock-wave Mach number, $\Delta\vartheta_{\mathrm{SW}}$ is the flow deflection induced by the shock wave, β_{SW} is the angle between the oblique shock wave and the incident flow, p_{t_∞} is the inflow total pressure, T_{t_∞} is the inflow total temperature, T_w is the wall temperature, T_r is the theoritical adiabatic wall-recovery temperature ($r_f = 0.89$), $T_{u_\infty} = \sqrt{(\frac{2}{3}k_\infty)}V_\infty^{-1}$ is the turbulence intensity at inflow, $\ell_{T_\infty} = k_\infty^{3/2}\varepsilon_\infty^{-1}$ is the turbulence length scale at inflow, δ_0 is the boundary-layer thickness at the beginning of the interaction,

$$\delta_0^* = \int_0^\delta \left(1 - \frac{\bar{\rho}\tilde{u}}{\bar{\rho}_\infty \tilde{u}_\infty}\right) \mathrm{d}y$$

is the boundary-layer displacement thickness at the beginning of the interaction,

$$\theta_0 = \int_0^\delta \frac{\bar{\rho}\tilde{u}}{\bar{\rho}_\infty \tilde{u}_\infty}\left(1 - \frac{\tilde{u}}{\tilde{u}_\infty}\right) \mathrm{d}y$$

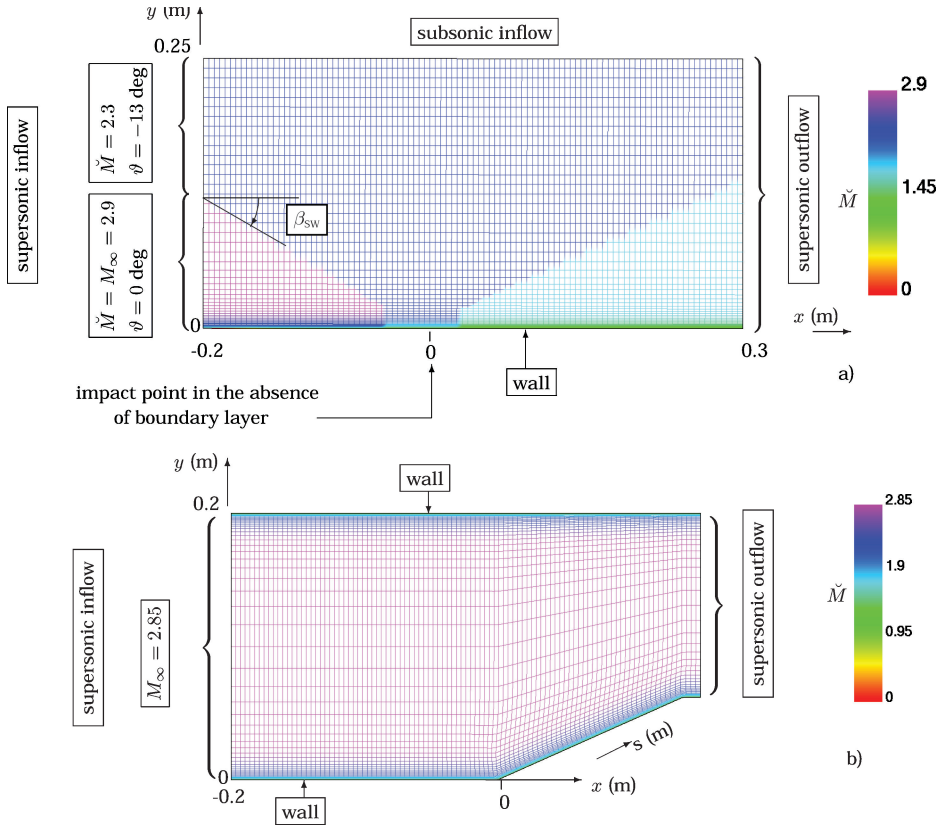

Fig. 1 Coarse computational grids, boundary conditions, and initial flowfield Mach number for a) incident-oblique-shock-wave interaction of Refs. 61–63, $M_\infty = 2.9$ and $Re_{\delta_0} = 0.97 \times 10^6$ and b) compression ramp of Refs. 64–67, $M_\infty = 2.85$ and $Re_{\delta_0} = 1.33 \times 10^6$.

Table 1 Configurations studied and grids required for grid convergence using different turbulence models

Parameter	Configuration		
	Reda–Murphy 13 deg	Settles 24 deg	Settles 20 deg
Source	Ref. 61	Refs. 64 and 65	Refs. 64 and 65
$M_\infty = M_{SW}$	2.9	2.85	2.85
$\Delta\vartheta_{SW}$ (deg)	13	24	20
β_{SW} (deg)	37.7	44	39
p_{t_∞} (Pa)	689,010	671,000	671,000
T_{t_∞} (K)	291	250	250
$\tilde{T}_w$ (K)	271	258.8	258.8
T_r (K)	270.9	233	233
T_{u_∞} %	1/–[a]	1/1[a]	1/1[a]
$\ell_{T_\infty} \times 10^3$ m	17[b]	25[b]	25[b]
$\delta_0 \times 10^3$ m	16.3/16.9[a]	20.2/21.1[a]	23.1/23.9[a]
$\delta_0^* \times 10^3$ m	3.7/3.9[a]	5.1/6.0[a]	6.7/7.3[a]
$\theta_0 \times 10^3$ m	0.82/0.82[a]	1.1/1.1[a]	1.4/1.2[a]
$Re_{\delta_0} \times 10^{-6}$	0.93/0.97[a]	1.43/1.33[a]	1.64/1.65[a]
$Re_{\delta_0^*} \times 10^{-5}$	2.1/2.2[a]	3.6/–[a]	4.8/–[a]
$Re_{\theta_0} \times 10^{-4}$	4.7/4.7[a]	7.9/8[a]	10/8[a]
$Re_\infty \times 10^{-7}$ m^{-1}	5.7	6.3	6.3
H_0	4.54	4.6	4.68
H_{k_0}	1.19	1.19	1.22
Π	0[c]	0.25[c]	0.65[c]
k–ε	grid_B	grid_B	grid_A
LSS RSM	grid_B	grid_B	grid_A
GV RSM	grid_C	grid_D	grid_B
WNF–LSS RSM	grid_B	grid_B	grid_A

[a]Computation/experiment. [b]Computation. [c]Inflow.

is the boundary-layer momentum thickness at the beginning of the interaction, $Re_{\delta_0} = V_\infty \delta_0 \breve{\nu}_\infty^{-1}$ is the boundary-layer thickness Reynolds number, $Re_{\delta_0^*} = V_\infty \delta_0^* \breve{\nu}_\infty^{-1}$ is the boundary-layer displacement-thickness Reynolds number, $Re_{\theta_0} = V_\infty \theta_0 \breve{\nu}_\infty^{-1}$ is the boundary-layer momentum-thickness Reynolds number; $Re_\infty = V_\infty \breve{\nu}_\infty^{-1}$ is the unit Reynolds number, $H_0 = \delta_0^* \theta_0^{-1}$ is the boundary-layer shape factor at the beginning of the interaction, $H_{k_0} = \delta_{k_0}^* \theta_{k_0}^{-1}$ is the kinematic boundary-layer shape factor

$$\left(\delta_{k_0}^* = \int_0^\delta \left(1 - \frac{\tilde{u}}{\tilde{u}_\infty}\right) \mathrm{d}y, \qquad \theta_{k_0} = \int_0^\delta \frac{\tilde{u}}{\tilde{u}_\infty}\left(1 - \frac{\tilde{u}}{\tilde{u}_\infty}\right) \mathrm{d}y\right)$$

Π is the Coles wake parameter used to define the inflow profile applied as boundary condition.[60]

The inflow boundary-layer profile was adjusted to obtain a close fit to the measured integral boundary-layer parameters at the beginning of the interaction, a procedure also followed by Rizzetta.[7] All of the computations were continued until full convergence of mean flow and Reynolds stresses and were carefully checked for grid convergence. Comparison of grid-converged results obtained using the two wall-normal free RSMs (GV and WNF–LSS), LSS RSM with geometric wall normals and wall distances, and the Launder–Sharma k–ε model, with measurements, are considered for assessing the models. These systematic comparisons are then analyzed to determine possible modeling improvements.

$M_{SW} = 2.9$ Incident Oblique Shock Wave[61]

This configuration consists of an oblique shock wave $M_{SW} = 2.9$ and $\Delta\vartheta_{SW} = 13$ deg impinging on a flat-plate turbulent boundary layer.[61–63] Experimental data include both wall-pressure[61] and skin-friction[62] distributions and laser Doppler velocimetry (LDV) measurements[63] of streamwise mean velocities $\bar{u}$ and turbulence fluctuations ($\overline{u'u'}$). Results are quite sensitive to both wall temperature and incoming boundary-layer shape factor.[60] Wall temperature, which was not measured, was fixed to $\tilde{T}_w = 271$ K, which is the expected adiabatic-wall temperature T_r for this configuration, assuming $\breve{M}_e = 2.9$ and a wall-temperature recovery factor $r_f = 0.89$. In the computations, the inflow boundary-layer profile was chosen (Table 1) to obtain, at the beginning of the shock-wave/boundary-layer interaction, the closest possible agreement of the integral boundary-layer parameters with measurements (Table 1). A similar strategy was adopted by Rizzetta.[7] The resulting agreement in Reynolds numbers Re_{θ_0} and $Re_{\delta_0^*}$ is excellent (Table 1).

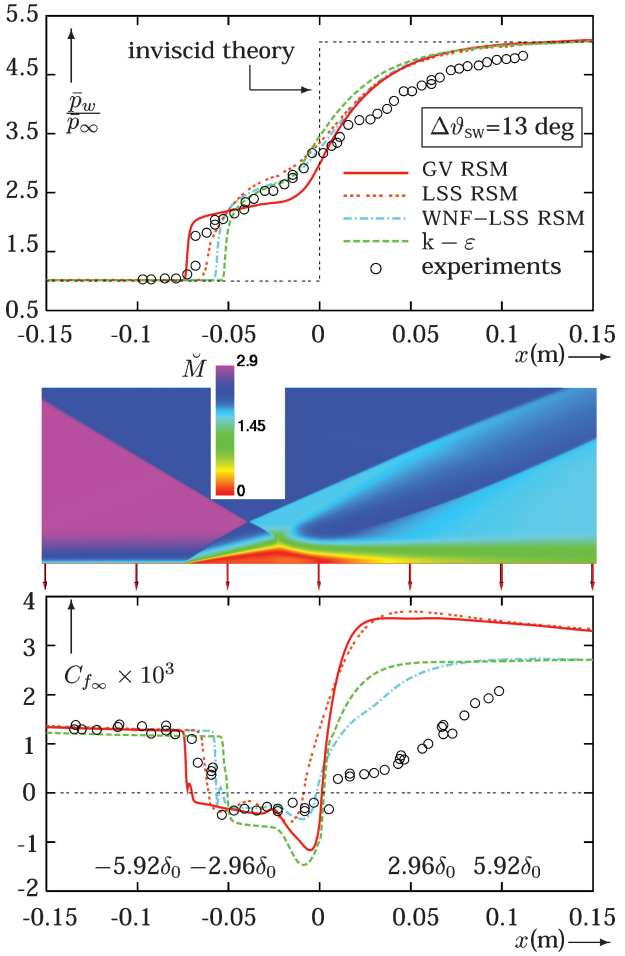

Fig. 2 Comparison of grid-converged computations (Table 1) with measurements[61,62] of wall pressure and skin-friction x-wise distributions, for Reda-Murphy[61] incident-shock-wave interaction, $M_\infty = 2.9$, $Re_{\delta_0} = 0.97 \times 10^6$, and $\Delta\vartheta_{SW} = 13$ deg using the GV[34] and WNF–LSS[35,36] RSMs, the LSS[50,51] RSM with geometric normals, and the Launder–Sharma[49] k–ε model (iso-Machs computed with the GV[34] RSM; grid_C).

Comparison of wall pressures (Fig. 2) indicates that the Launder–Sharma[49] k–ε computations give the worst prediction of upstream influence. The use of the Launder–Shima RSM with geometric wall-topography parameters (LSS[51]) substantially improves the prediction of upstream influence, which is slightly underestimated. The GV[34] wall-normal free RSM slightly overestimates upstream influence consistently with evidence from other complex flows,[35,36] where it is known to overpredict separation slightly. The WNF version of the Launder–Shima[50] RSM (WNF–LSS[35]) underpredicts upstream influence, but note that it performs better than the k–ε model.

Considering the skin-friction distribution (Fig. 2), notice that the three RSMs predict the correct level of wall friction in the separated flow region (at a value of -0.44×10^{-3}) contrary to the k–ε result, which overestimates negative friction (to a value of -0.7×10^{-3}). This is an interesting result especially because skin-friction was directly measured using flush-mounted strain-gauges,[62] giving detailed experimental data in the separated flow region. The behavior at reattachment is quite interesting. The WNF–LSS[35] RSM gives the best results compared to the other models.

It is significant that this WNF version of the LSS[50,51] model (WNF–LSS[35]) gives substantially better results than the corresponding model with geometric normals. It has been consistently observed that WNF models developed using the WNF methodology suggested by the authors[35] improve on the corresponding models with wall normals.

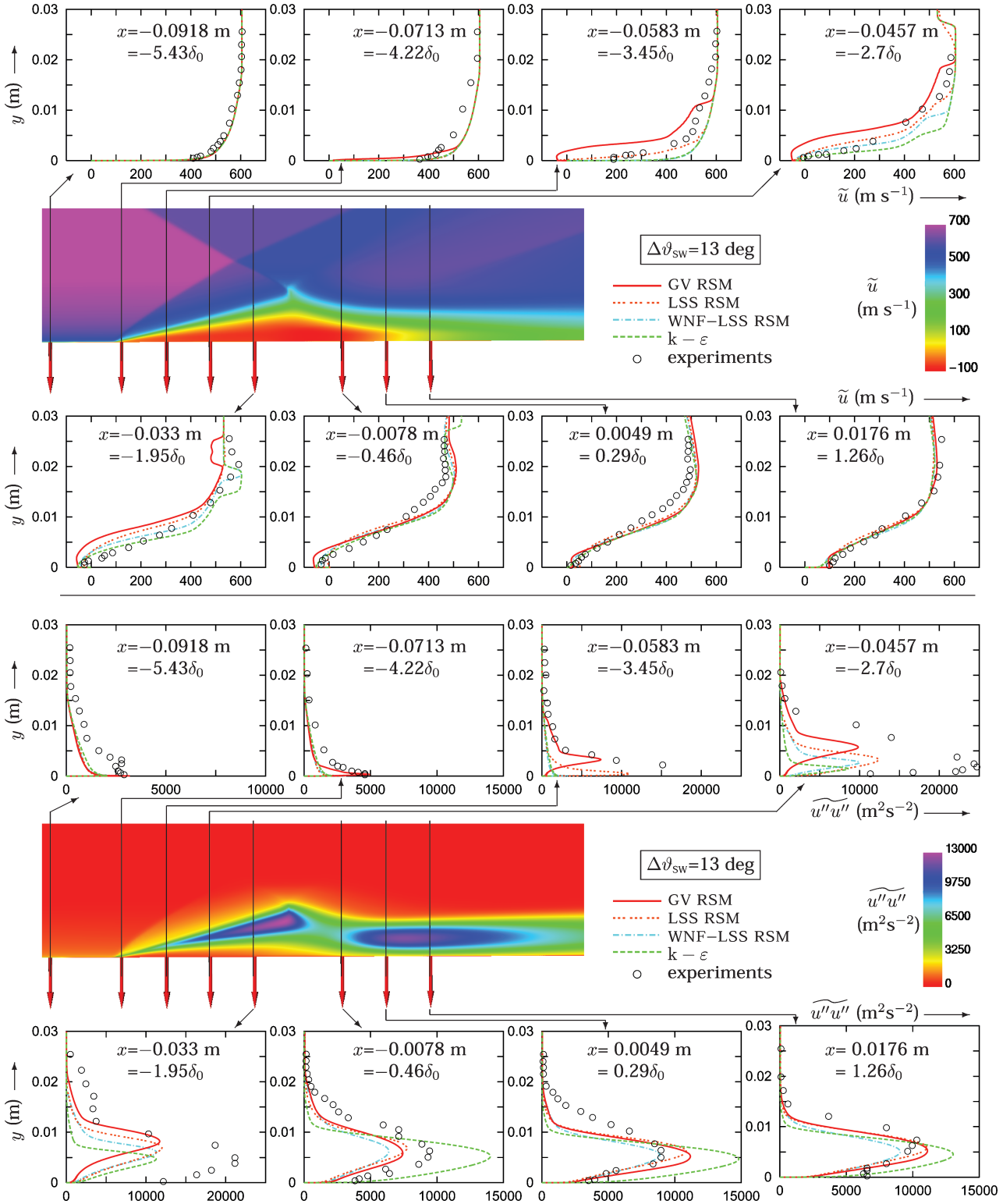

Fig. 3 Comparison of grid-converged computations (Table 1) with measurements[61,62] of mean velocity ($\tilde{u}$, $\bar{u}$) and velocity fluctuations ($\widetilde{u''u''}$, $\overline{u'u'}$) at various axial stations for Reda–Murphy[61] (Table 1) incident-shock-wave interaction, $M_\infty = 2.9$, $Re_{\delta_0} = 0.97 \times 10^6$, and $\Delta\vartheta_{SW} = 13$ deg, using the GV[34] and WNF–LSS[35,36] RSMs, the LSS[50,51] RSM with geometric normals, and the Launder–Sharma[49] k–ε model (iso-$\tilde{u}$ and iso-$\widetilde{u''u''}$ computed with the GV[34] RSM; grid_C).

Computed streamwise Favre-averaged mean velocities $\tilde{u}$ are compared with LDV-measured[63] Reynolds averaged velocities $\bar{u}$, at various x-wise stations (Fig. 3). Overall agreement is quite satisfactory and consistent with the predicted upstream-influence and reattachment behavior, the GV[34] model separating slightly earlier than others and the k–ε slightly later. Also note that all models give similar results, in good agreement with measurements after reattachment (Fig. 3; $x = 1.26\delta_0$).

Comparison of computed streamwise Reynolds stress $\widetilde{u''u''}$ with LDV-measured[63] values ($\overline{u'u'}$) clearly indicates the superiority of RSMs compared to k–ε (Fig. 3), which is of course expected. In the initial (separating) part of the interaction ($x = -4.22\delta_0$, $-3.45\delta_0$) the GV RSM closure[34] gives the best prediction. Within the separated region, all models underestimate the $\widetilde{u''u''}$ peak by almost a factor two. This is often the case in shock-wave/boundary-layer interactions, with virtually every Reynolds average Navier–Stokes

model. In a recent work, Chassaing et al.[68] have shown that this can be related to low-frequency oscillations eventually present in the experimental flow. Such oscillations, if present, will be considered as turbulence by the experimental averaging procedure and could explain this frequently observed underestimation of turbulence peak in the computations, although highly resolved LES computations are necessary to clarify this point. In the reattachment region, the turbulence levels predicted by the RSMs are quite satisfactory, whereas the k–ε model overestimates these levels.

A discussion concerning the difference observed between the three RSM models is necessary because it can direct future modeling work. There are two main differences between the two WNF RSMs: 1) the rapid redistribution term coefficient dependence on the Reynolds stress anisotropy-tensor flatness parameter A, where the WNF–LSS[35,36] (and the original LSS[50,51] model with geometric normals) follow a function suitable for the log-layer and equilibrium turbulence ($C_2^H = 0.75\sqrt{A}$), whereas the GV[34] RSM has been designed to separate by sharply increasing C_2^H when $A > 0.55$, and 2) the turbulent diffusion model, where the GV[34] model uses the Hanjalić–Launder[59] model for turbulent diffusion, whereas the WNF–LSS[35,36] (and the original LSS[50,51] model with geometric normals) use the Daly–Harlow[58] turbulent diffusion model.

As far as separation (upstream influence) is concerned, the GV[34] model slightly overseparates, whereas the WNF–LSS[35,36] underpredicts separation, consistently with the C_2^H design of the model (Fig. 2). Comparison of the WNF–LSS[35,36] model with the corresponding LSS[50,51] model with wall normals indicates that the WNF model separates slightly less.

Consideration of the skin-friction distribution (Fig. 2) highlights the improvement brought by the use of WNF models (WNF–LSS[35,36] vs LSS[50,51]). The difference between the two WNF models is more subtle. A systematic study on the influence of diffusion modeling[35] demonstrates that the difference in C_{f_∞} at the reattachment and relaxation region between the GV[34] and WNF–LSS[35,36] RSMs is mainly caused by the different turbulent diffusion model used. Consideration of a number of flows[35] tends to indicate that the Daly–Harlow[58] model improves the near-wall (C_{f_∞}) separation and reattachment behavior, whereas the Hanjalić–Launder[59] model performs better at the boundary-layer edge. (Boundary-layer entrainment is better predicted.)

To substantiate the preceding comparisons, a careful grid convergence study had been previously conducted (Fig. 4) using the two WNF RSMs. All of the grids studied in the present work (Table 2) had the same grid cell size at the wall ($y_w^+ < 0.3$). In Table 2, i and j indicate grid directions, N_i and N_j are the number of points, y_w^+ is the nondimensional distance of the first grid node away from the wall, r_j is geometric progression ratio, and L_x and L_y are lengths. A separate study, not shown here, has shown that reducing this size

Table 2 Computational grids used

Grid	$N_i(N_x)$	$N_j(N_y)$	N_{j_s}	r_j	$y_w^+ = n_w^+$	L_x, m	L_y, m
			Reda–Murphy 13 deg				
grid_D	1201	1201	961	1.0085	0.3	0.5	0.25
grid_C	801	801	641	1.0134	0.3		
grid_B	401	401	321	1.0295	0.3		
grid_A	201	201	161	1.065	0.3		
			Settles 20–24 deg				
grid_E	1601	1601	801	1.011	0.3	0.31524	0.2
grid_D	1201	1201	601	1.015	0.3		
grid_C	801	801	401	1.0237	0.3		
grid_B	601	601	301	1.032	0.3		
grid_A	401	201	101	1.1176	0.3		

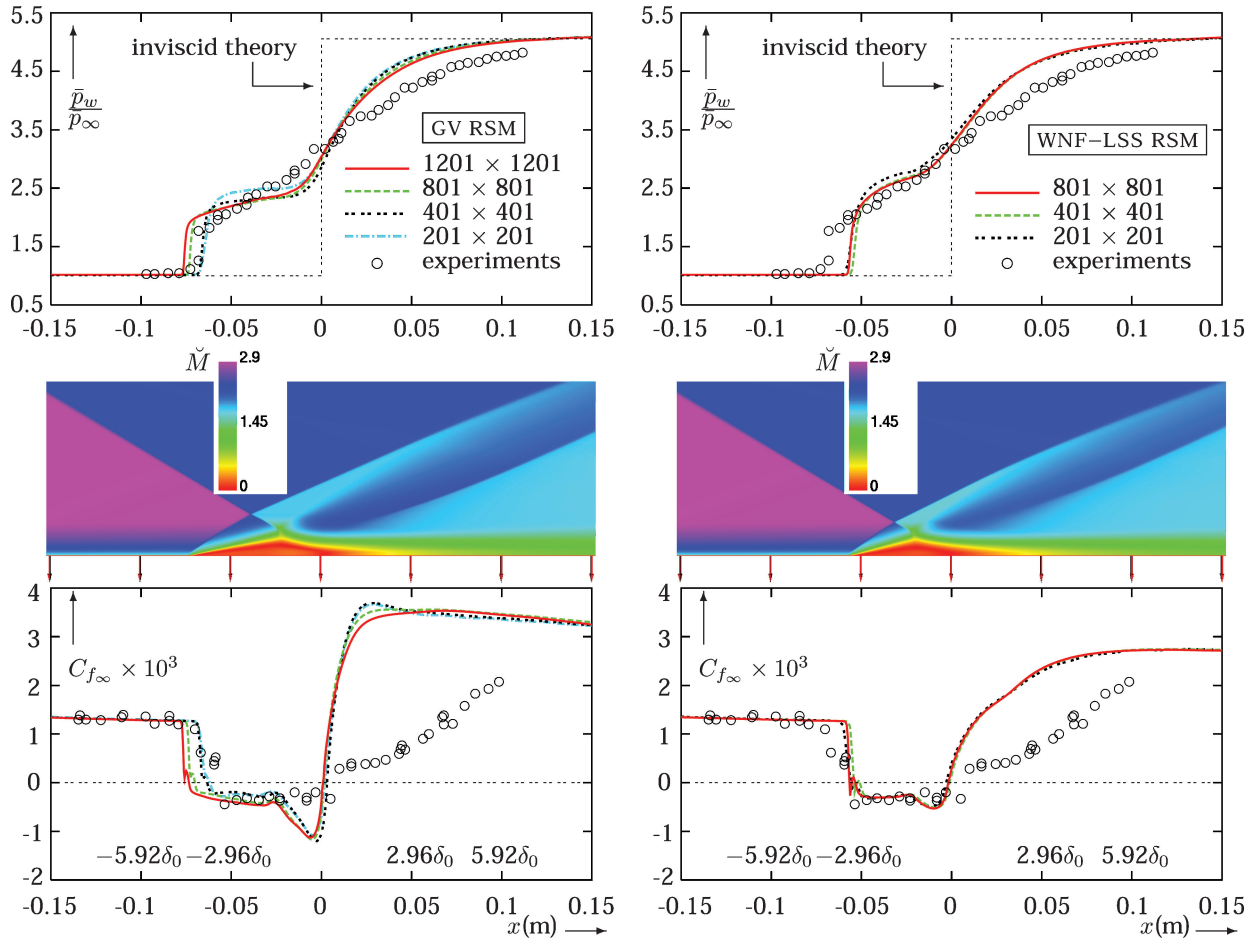

Fig. 4 Grid convergence study for the Reda–Murphy[61] (Table 1) incident-shock-wave interaction, $M_\infty = 2.9$, $Re_{\delta_0} = 0.97 \times 10^6$, and $\Delta\vartheta_{SW} = 13$ deg using various grids (Table 2) and the two WNF RSMs (GV[34], grid_C; and WNF–LSS[35,36], grid_B).

to $y_w^+ < 0.15$ did not alter the results (either for wall pressure or skin friction). The different grids used were progressively refined both x-wise ($\Delta x = \text{const}$) and y-wise. The y-refinement aimed at increasing grid resolution in the entire boundary layer (including the outer-edge entrainment zone). For the WNF–LSS[35,36] model, which predicts a less extended separation, grid convergence is quit rapid (Fig. 4). The initial 201×201 grid_A gives the correct upstream-interaction length, and the 401×401 grid_B is sufficient to obtain grid-converged results. The GV[34] RSM predicts a larger separation, and as a consequence, finer grid resolution is required farther away from the wall compared to the WNF–LSS[35,36] model. As a result, a 801×801 grid_C (Table 2) is necessary to obtain fully grid-converged results. Similar grid convergence studies have been performed for all of the turbulence models used and for all the configurations, to define the grid on which the grid-converged results are presented (Table 1).

Table 3 Particular frames used in the compression-ramp experimental setup[64–67]

	α_{exp}		
α_c, deg	0 deg	5.5 deg	α_c
20	$s \le -0.0127$ m	$-0.0127 < s \le 0.0127$ m	$s > 0.0127$ m
24	——	$s \le 0.01016$ m	$s > 0.01016$ m

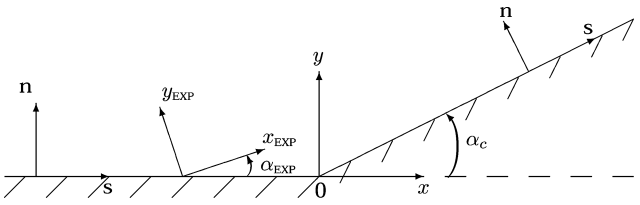

Fig. 5 Various frames used in the compression-ramp experimental setups: (x, y) is Cartesian reference frame (x aligned with the incoming flow); (s, n) are curvilinear coordinates (s along the wall and n normal to the wall direction); and $(x_{\text{exp}}, y_{\text{exp}})$ is particular frame used in Refs. 64–67 to quasi align x_{exp} with the main velocity direction within the boundary layer.

$M_{SW} = 2.85$ Compression Ramps[64–67]

The configuration of Refs. 64–67 consists of a number of compression ramps, in a $M_\infty = 2.85$ stream, and in the present work the two higher ramp angles for which extended flow separation was observed ($\alpha_c = 20$ and 24 deg) were computed. Measurements include wall-pressure, wall-friction (Preston tube measurements), and wall-temperature distributions,[64,65] and profile measurements of $\breve{p}_t$, $\bar{p}$, and $\breve{T}_t$, which were used to deduce mean flow velocities. Because of the measurement procedure used ($\breve{p}_t$, $\bar{p}$, and $\breve{T}_t$), it seems plausible to assume that the modulus of velocity, $|\tilde{V}| = \sqrt{(\tilde{u} + \tilde{v})}$, was obtained and was subsequently attributed a negative sign in the separated flow region where the probes were turned to face the backflow.[65,66] The profiles were measured in an ad-hoc local frame (x_{exp}, y_{exp}), which was defined (Fig. 5 and Table 3) to have y_{exp} roughly perpendicular to the zero-velocity line in the separated flow region. Wall temperature was fixed to $\tilde{T}_w = 258.8$ K in accordance with measurements.[64,65] Again the inflow boundary-layer profile was chosen to fit correctly the measured integral parameters at the beginning of the interaction (Table 1). Agreement is excellent for the $\alpha_c = 24$ deg case but could be improved for the $\alpha_c = 20$ deg case.

Comparison of grid-converged computations, using the four turbulence models, for wall pressure and wall shear,[64,65] shows (Fig. 6)

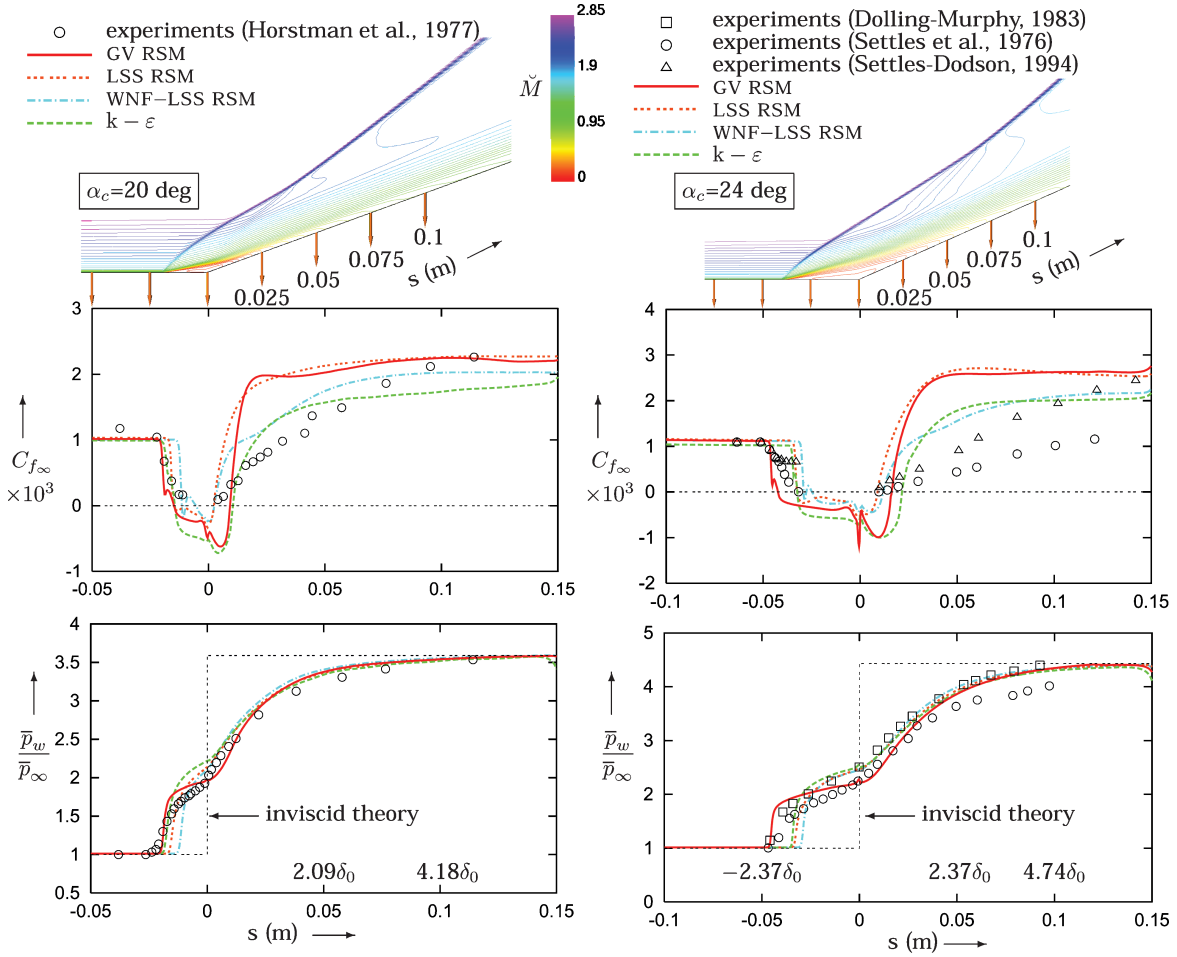

Fig. 6 Comparison of grid-converged computations (Table 1) with measurements[64–67] of wall-pressure and skin-friction s-wise distributions, for the $\alpha_c = 20$ and 24 deg (Refs. 64–67) compression-ramp interactions, $M_\infty = 2.85$ and $Re_{\delta_0} = 1.33$–1.65×10^6, using GV[34] and WNF–LSS[35,36] RSMs, the LSS[50,51] RSM with geometric normals, and the Launder–Sharma[49] k–ε model (Mach contours computed with GV[34] RSM; grid_D).

that the GV[34] RSM gives the best prediction of upstream influence and of the separation point. The WNF–LSS[35,36] model underestimates upstream influence but gives the best prediction of skin friction at reattachment and in the relaxation region. Note in particular that only the WNF–LSS[35,36] RSM captures the experimentally observed inflection of the C_{f_∞} distribution in the relaxation region for both ramp angles (Fig. 6) and gives the correct value of C_{f_∞} (taking into account experimental accuracy) at the end of the interaction. For the $\alpha_c = 24$ deg ramp, many measurements have been accumulated over the years[66,67] and two sets of $\bar{p}_w$ and C_{f_∞} data were included to give an estimation of experimental repeatability for this difficult flow. (The second set of C_{f_∞} data[67] was found in the Settles and Dodson database,[67] again from Preston tube measurements, but the exact source is not given.)

Comparison of grid-converged computations and measured mean-velocity modulus [$\mathrm{sign}(\tilde{u})|\tilde{V}|$ vs $y_{\exp}$] (Fig. 5) using the four

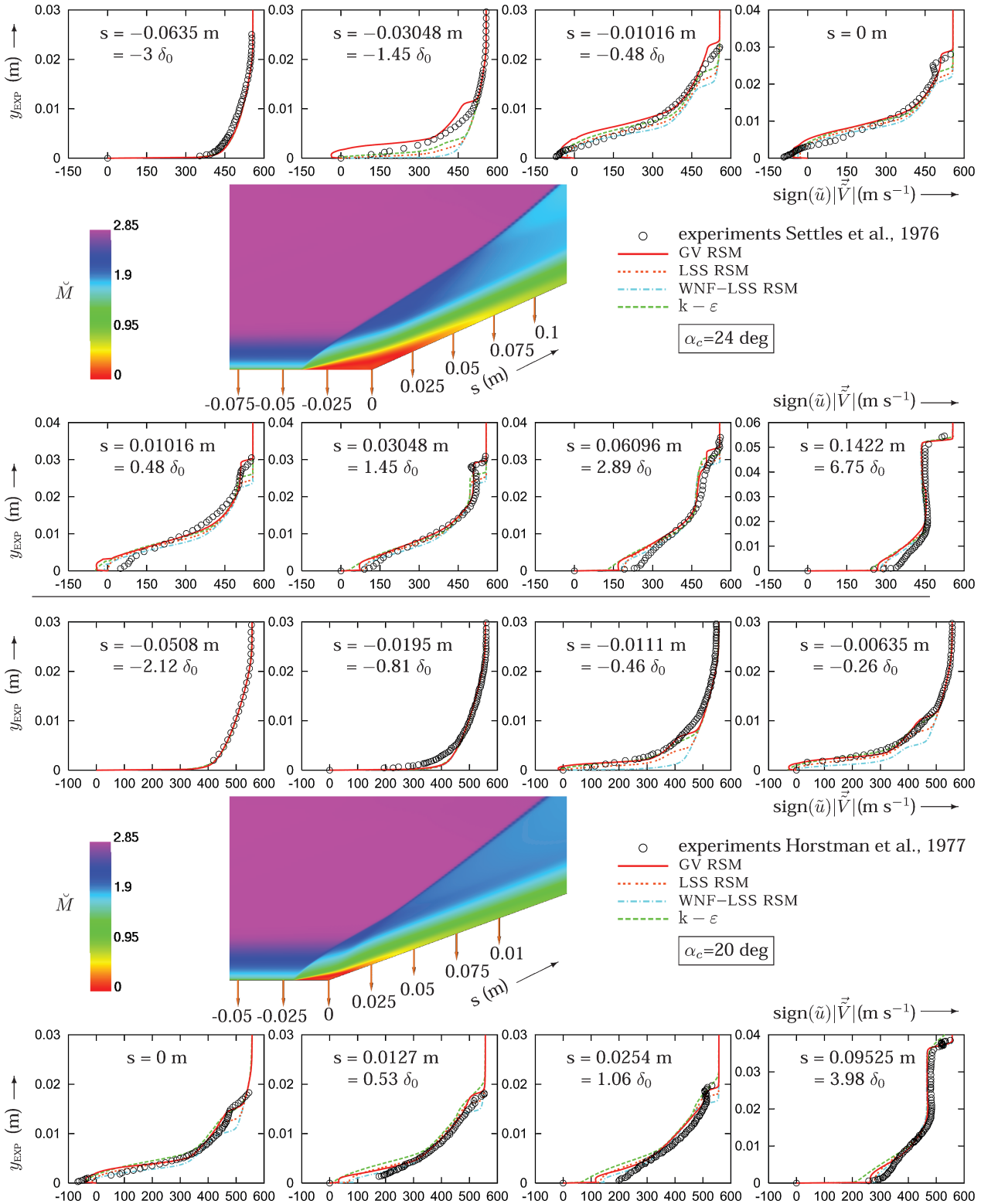

Fig. 7 Comparison of grid-converged computations (Table 1) with measurements[64–67] of mean-velocity modulus [$\mathrm{sign}(\tilde{u})|\tilde{V}|$] at various axial stations, for the $\alpha_c = 20$ and 24 deg (Refs. 64–67) compression-ramp interactions, $M_\infty = 2.85$ and $Re_{\delta_0} = 1.33$–1.65×10^6 using the GV[34] and WNF–LSS[35,36] RSMs, the LSS[50,51] RSM with geometric normals, and the Launder–Sharma[49] k–ε model (iso-Machs computed with GV[34] RSM; grid_D).

turbulence models, for the 2 ramp-angles ($\alpha_c = 20$ deg and 24 deg) (Fig. 7) is consistent with the wall-pressure and skin-friction comparisons (Fig. 6).

For the $\alpha_c = 20$ deg ramp, it is seen (Fig. 7) that the agreement with measurements before the interaction ($s \cong -2\delta_0$) is quite satisfactory, in agreement with integral boundary-layer parameters (Table 1). The GV[34] RSM predicts the correct position of separation (Fig. 7, $s = -0.46\delta_0$), whereas the WNF–LSS[35,36] RSM separates a little latter. In the reattachment region, the WNF–LSS[35,36] gives the best results in agreement with the C_{f_∞} results (Fig. 6).

For the $\alpha_c = 24$ deg case, analogous conclusions can be drawn, although the computed profile at the beginning of the interaction is a bit too full (Table 1). At $s = -1.45\delta_0$, the GV[34] RSM has already separated, whereas the other models have not separated yet (Fig. 7). However, this is not significant because of the variations observed in wall-pressure distributions between various experimental campaigns (Fig. 6). The GV[34] results agree well with the pressure distribution measured by Dolling and Murphy[66] (Fig. 6). The experimentally measured upstream influence in the Dolling and Murphy campaign[66] was larger than in the Settles et al.[64] campaign in which the velocity measurements were obtained (Fig. 7). All of the other models, however, separate a little late (Figs. 6 and 7).

A grid-convergence study was conducted with both models (Fig. 8), using various grids (Table 2). Results with both models are quite near grid-convergence on the initial 401×201 grid_A (Table 2), although full grid convergence is achieved on the 601×601 grid_B for the WNF–LSS[35,36] RSM, to resolve a slight difference in C_{f_∞} at $s \cong 0.04$ m (Fig. 8) and on the 1201×1201 for the GV[34] RSM.

Turbulence Modeling Issues

Before drawing conclusions, one should bear in mind some inherent difficulties associated with the experimental characterization of oblique-shock-wave/turbulent-boundary-layer interaction flows: 1) Three-dimensional effects are certainly present in the experimental setup, as has been indicated by Reda and Murphy[69] for the incident shock-wave configuration and to a lesser extent in the $\alpha_c = 24$ deg ramp case (where the use of aerodynamic fences reduces three-dimensional effects[64]), biasing the upstream-influence length estimation, and 2) the exact repeatability of the experimental flow is a very difficult task, as witnessed by the scatter of experimental wall-pressure data and inflow boundary-layer integral parameters[64–67] for the $\alpha_c = 24$ deg compression ramp case.

This note of caution notwithstanding, a general impression from the comparison with experimental results presented is that the proposed WNF RSMs (GV and WNF–LSS) give satisfactory results, often better than previous RSMs with geometric wall normals and better than the standard k–ε, especially if one is interested in detailed turbulence field description. This is important because other suggested alternatives to Boussinesq closures, such as EARSM, often give unsatisfactory results.[3–8]

It can be concluded that the GV[34] RSM is the one that has a marked tendancy to separate. (The coefficient C_2^H of the rapid redistribution closure was designed to do so.) On the other hand, the WNF–LSS[35,36] RSM underpredicts separation because it uses the C_2^H coefficient of the basic LSS[50] RSM that is only suitable for equilibrium flows. However the WNF–LSS[35,36] (which is a WNF version of the basic LSS[50,51] RSM) performs very well at the reattachment

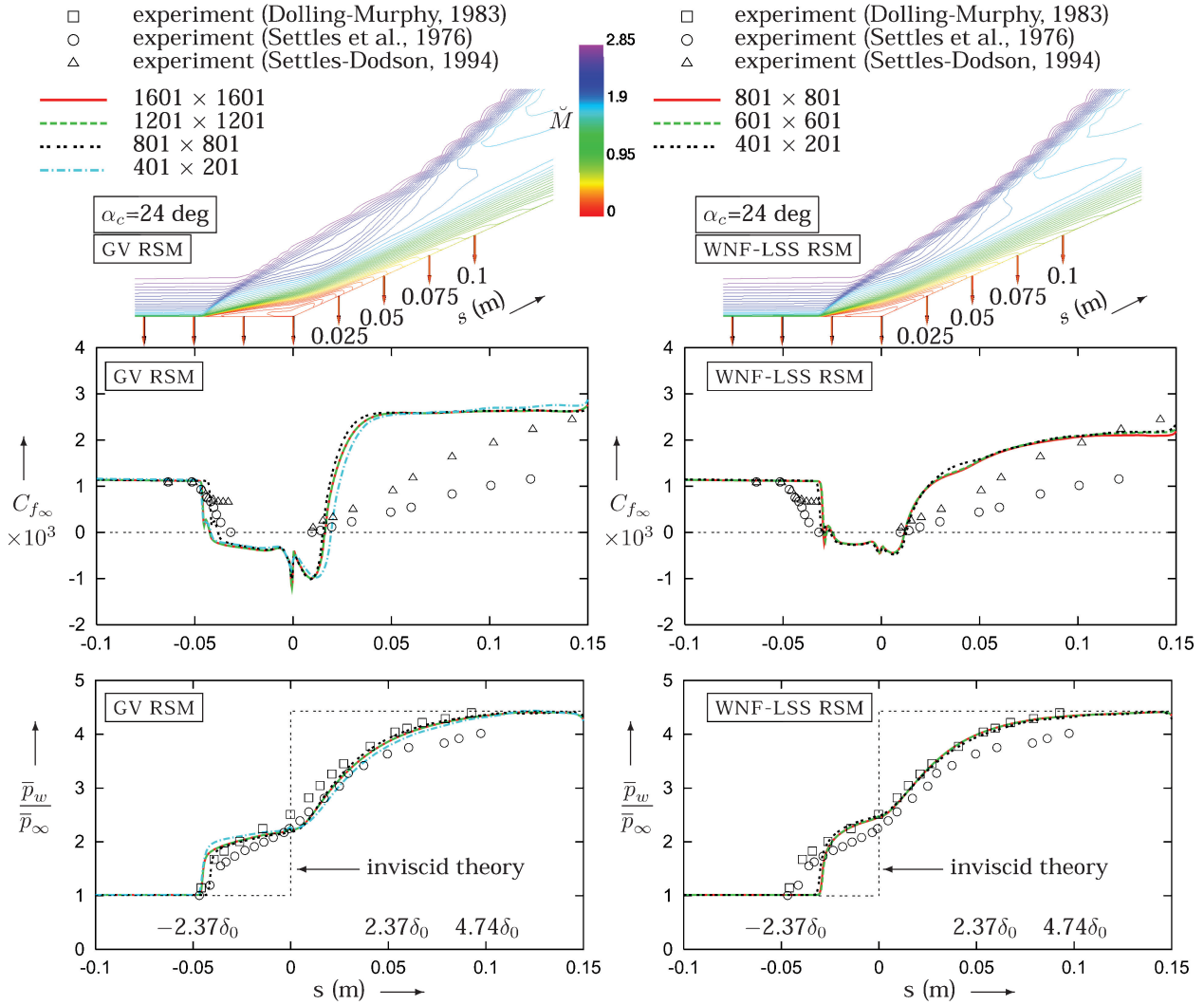

Fig. 8 Grid-convergence study of wall-pressure and skin-friction s-wise distributions, for the $\alpha_c = 24$ deg (Refs. 64, 65, and 67) compression-ramp interaction, $M_\infty = 2.85$ and $Re_{\delta_0} = 1.33 \times 10^6$ (Table 1), using GV[34] and WNF–LSS[35,36] RSMs, on various grids (Table 2) (Mach contours computed with grid_A).

and downstream relaxation, especially concerning the prediction of skin friction. This difference between the two wall-normal-free RSMs is attributed to the different closure used for the turbulent diffusion.[35,36] These remarks are consistent with other experimental validations of these models.[35,36,40]

Conclusions

Near-wall WNF RSMs are at a stage of development where they allow for robust modeling of complex flows, being applicable to arbitrary geometries because of their complete independence of any wall-topology-related parameters. Comparison of grid-converged computations with measurements for three oblique-shock-wave/turbulent-boundary-layer interactions ($M_\infty = 2.85 - 2.9$ and $Re_{\delta_0} = 0.97 - 1.65 \times 10^6$) indicate that the GV RSM slightly overpredicts separation, whereas the WNF–LSS RSM slightly underpredicts it. For the present comparisons, and in other published comparisons for complex three-dimensional flows, it seems that an improved model should give results between these two models, and current modeling work aims to 1) improve the $C_2^H(A)$ function used for the quasi-linear isotropization of production closure for the rapid pressure–strain, with the aim to predict separation between the two models, and 2) develop an improved turbulent diffusion model that will combine the advantages of an Hanjalić–Launder-type closure at the boundary-layer edge with the remarkable improvement in skin-friction prediction associated with the use of a Daly–Harlow turbulent diffusion model near the wall.

Note that the WNF–LSS RSM closure improves on the corresponding closure that used wall normals (LSS RSM), so that rendering an existing RSM model WNF using the proposed inhomogeneity direction unit vector not only allows for easy implementation in complex geometries, but also improves on the results of the initial model. Finally, the k–ε model results, consistent with previous work by many authors, not only underestimate separation and upstream interaction length, but also overpredict negative skin friction and give an unsatisfactory prediction of the Reynolds stresses field.

Acknowledgments

This work was partly supported by Project T0216-0219 of the Supersonic Research Initiative of the French Ministry of Research, coordinated by A. Lerat. The computations presented in this work were run at the Institut pour le Développement des Ressources en Informatique Scientifique, where computer resources were made available by the Comité Scientifique. The authors are listed alphabetically.

References

[1]Délery, J. M.,"Shock Wave/Turbulent Boundary Layer Interaction and its Control," *Progress in Aerospace Science*, Vol. 22, 1985, pp. 205–280.

[2]Dolling, D. S., "Fifty Years of Shock-Wave/Boundary-Layer Interaction Research: What Next?," *AIAA Journal*, Vol. 39, No. 8, 2001, pp. 1517–1531.

[3]Viegas, J. R., and Horstman, C. C., "Comparison of Multiequation Turbulence Models for Several Shock Boundary-Layer Interaction Flows," *AIAA Journal*, Vol. 17, No. 8, 1979, pp. 811–820.

[4]Knight, D. D., Horstman, C. C., and Bogdonoff, S., "Structure of Supersonic Turbulent Flow Past a Swept Compression Corner," *AIAA Journal*, Vol. 30, No. 4, 1992, pp. 890–896.

[5]Thivet, F., Knight, D. D., Zheltovodov, A. A., and Maksimov, A. I., "Analysis of Observed and Computed Crossing-Shock-Wave/Turbulent-Boundary-Layer Interactions," *Aerospace Science and Technology*, Vol. 2002·6, 2002, pp. 3–17.

[6]Liou, W. W., Huang, G., and Shih, T. H., "Turbulence Model Assessment for Shock-Wave/Turbulent-Boundary-Layer Interaction in Transonic and Supersonic Flows," *Computers and Fluids*, Vol. 29, 2000, pp. 275–299.

[7]Rizzetta, D. P., "Evaluation of Explicit Algebraic Reynolds-Stress Models for Separated Supersonic Flows," *AIAA Journal*, Vol. 36, No. 1, 1998, pp. 24–30.

[8]Goldberg, U. G., Batten, P., Palaniswamy, S., Chakravarthy, S., and Peroomian, O., "Hypersonic Flow Prediction Using Linear and Nonlinear Turbulence Closures," *Journal of Aircraft*, Vol. 37, No. 4, 2000, pp. 671–675.

[9]Speziale, C. G., and Abid, R., "Near-Wall Integration of Reynolds Stress Turbulence Closure with No Wall Damping," *AIAA Journal*, Vol. 33, No. 10, 1995, pp. 1974–1977.

[10]Shih, T.-H., Liou, W. W., Shabbir, A., Yang, Z., and Zhu, J., "A New k–ε Eddy Viscosity Model for High Reynolds Number Turbulent Flows," *Computers and Fluids*, Vol. 24, No. 3, 1995, pp. 227–238.

[11]Urbin, G., and Knight, D., "Large-Eddy Simulation of a Supersonic Boundary Layer Using an Unstructured Grid," *AIAA Journal*, Vol. 39, No. 7, 2001, pp. 1288–1295.

[12]Rizzetta, D. P., Visbal, M. R., and Gaitonde, D. V., "Large-Eddy Simulation of Supersonic Compression-Ramp Flow by High-Order Method," *AIAA Journal*, Vol. 39, No. 12, 2001, pp. 2283–2292.

[13]Rizzetta, D. P., and Visbal, M. R., "Application of Large-Eddy Simulation to Supersonic Compression Ramps," *AIAA Journal*, Vol. 40, No. 8, 2002, pp. 1574–1581.

[14]Garnier, E., Sagaut, P., and Deville, M., "Large-Eddy Simulation of the Shock/Boundary-Layer Interaction," *AIAA Journal*, Vol. 40, No. 10, 2002, pp. 1935–1944.

[15]Wilcox, D. C., and Rubesin, W., "Progress in Turbulence Modeling for Complex Flow Field Including Effect of Compressibility," NASA TP 1517, April 1980.

[16]Wilcox, D. C., "Multiscale Model for Turbulent Flows," *AIAA Journal*, Vol. 26, No. 11, 1988, pp. 1311–1320.

[17]Wilcox, D. C., "Supersonic Compression-Corner Applications of a Multiscale Model for Turbulent Flows," *AIAA Journal*, Vol. 28, No. 7, 1990, pp. 1194–1198.

[18]Wilcox, D. C., *Turbulence Modelling for CFD*, DCW Industries, Inc, 1998, pp. 294–296, 323–330.

[19]Lee, J., Taulbee, D. B., and Holden, M. S., "Study of Turbulence on Supersonic Compression Surfaces Using Reynolds Stress Model," *AIAA Journal*, Vol. 30, No. 7, 1992, pp. 1738–1746.

[20]Ladiende, F., "Supersonic Flux-Split Procedure for Second Moments of Turbulence," *AIAA Journal*, Vol. 33, No. 7, 1995, pp. 1185–1195.

[21]Launder, B. E., Reece, G. J., and Rodi, W., "Progress in the Development of a Reynolds-Stress Turbulence Closure," *Journal of Fluid Mechanics*, Vol. 68, 1975, pp. 537–566.

[22]Pantano, C., and Sarkar, S., "A Study of Compressibility Effects in the High-Speed Turbulent Shear Layer Using Direct Simulation," *Journal of Fluid Mechanics*, Vol. 451, 2002, pp. 329–371.

[23]Morrison, J. H., Gatski, T. B., Sommer, T. P., Zhang, H. S., and So, R. M. C., "Evaluation of a Near-Wall Turbulent Closure Model in Predicting Compressible Ramp Flows," *Near-Wall Turbulent Flows*, edited by R. M. C. So, C. G. Speziale, and B. E. Launder, Elsevier, New York, 1993, pp. 239–250.

[24]Zhang, H. S., So, R. M. C., Gatski, T. B., and Speziale, C. G., "A Near-Wall Second-Order Closure for Compressible Turbulent Flows," *Near-Wall Turbulent Flows*, edited by R. M. C. So, C. G. Speziale, and B. E. Launder, Elsevier, New York, 1993, pp. 209–218.

[25]Chenault, C. F., and Beran, P. S., "k–ε and Reynolds Stress Turbulence Model Comparisons for Two-Dimensional Injection Flows," *AIAA Journal*, Vol. 36, No. 8, 1998, pp. 1401–1412.

[26]Chenault, C. F., Beran, P. S., and Bowersox, R. D. W., "Numerical Investigation of Supersonic Injection using a Reynolds-Stress Turbulence Model," *AIAA Journal*, Vol. 37, No. 10, 1999, pp. 1257–1269.

[27]Sommer, T. P., So, R. M. C., and Zhang, H. S., "Supersonic Flow Calculations using a Reynolds-Stress and a Thermal Eddy Diffusivity Turbulence Model," *Journal of Fluids Engineering*, Vol. 116, 1994, pp. 469–476.

[28]Zha, G.-C., and Knight, D., "Three-Dimensional Shock/Boundary-Layer Interaction Using Reynolds Stress Equation Turbulence Model," *AIAA Journal*, Vol. 34, No. 7, 1996, pp. 1313–1320.

[29]Gnedin, M., and Knight, D., "A Reynolds Stress Equation Turbulence Model for Compressible Flows. Part I: Flat Plate Boundary Layers," AIAA Paper 95-0860, Jan. 1995.

[30]Batten, P., Craft, T. J., Leschziner, M. A., and Loyau, H., "Reynolds-Stress-Transport Modeling for Compressible Aerodynamics Applications," *AIAA Journal*, Vol. 37, No. 7, 1999, pp. 785–797.

[31]Barakos, G., and Drikakis, D., "Investigation of Nonlinear Eddy-Viscosity Turbulence Models in Shock/Boundary-Layer Interaction," *AIAA Journal*, Vol. 38, No. 3, 2000, pp. 461–469.

[32]Rumsey, C. L., Gatski, T. B., and Morrison, J. H., "Turbulence Model Predictions of Strongly Curved Flow in a U-Duct," *AIAA Journal*, Vol. 38, No. 8, 2000, pp. 1394–1402.

[33]Launder, B. E., and Li, S. P., "On the Elimination of Wall-Topography Parameters from 2-Moment Closure," *Physics of Fluids*, Vol. 6, 1994, pp. 999–1006.

[34]Gerolymos, G. A., and Vallet, I., "Wall-Normal-Free Near-Wall Reynolds-Stress Closure for Three-Dimensional Compressible Separated Flows," *AIAA Journal*, Vol. 39, 2001, pp. 1833–1842.

[35]Gerolymos, G. A., Sauret, E., and Vallet, I., "Contribution to the Single-Point-Closure Reynolds-Stress Modelling of Inhomogeneous Flow," *Theoretical and Computational Fluid Dynamics* (to be published).

[36]Gerolymos, G. A., and Vallet, I., "Contribution to Single-Point-Closure Reynolds-Stress Modelling of Inhomogeneous Flow," American Society of Mechanical Engineers, ASME Paper FEDSM2003-45346, July 2003.

[37]So, R. M. C., and Yuan, S. P., 1999, "A Geometry Independent Near-Wall Reynolds-Stress Closure," *International Journal of Engineering Science*, Vol. 37, 1999, pp. 33–57.

[38]Chassaing, J. C., Gerolymos, G. A., and Vallet, I., "Efficient and Robust Reynolds-Stress Model Computation of Three-Dimensional Compressible Flows," *AIAA Journal*, Vol. 41, No. 5, 2003, pp. 763–773.

[39]Chassaing, J.-C., Gerolymos, G. A., and Vallet, I., "Reynolds-Stress Model Dual-Time-Stepping Computation of Unsteady Three-Dimensional Flows," *AIAA Journal*, Vol. 41, No. 10, 2003, pp. 1882–1894.

[40]Gerolymos, G. A., and Vallet, I., "Wall-Normal-Free Reynolds-Stress Model for Three-Dimensional Turbomachinery Flows," *AIAA Journal*, Vol. 40, No. 2, 2002, pp. 199–208.

[41]Gerolymos, G. A., Neubauer, J., Sharma, V. C., and Vallet, I., "Improved Prediction of Turbomachinery Flows using Near-Wall Reynolds-Stress Model," *Journal of Turbomachinery*, Vol. 124, 2002, pp. 86–99.

[42]Gerolymos, G. A., Neubauer, J., and Michon, G. J., "Analysis and Application of Chorochronic Periodicity for Turbomachinery Rotor/Stator Interaction Computations," *Journal of Propulsion and Power*, Vol. 18, 2002, pp. 1139–1152.

[43]Chou, P. Y., "On Velocity Correlation and the Solution of the Equations of Turbulent Fluctuations," *Quarterly of Applied Mathematics*, Vol. 3, 1945, pp. 38–54.

[44]Lumley, J. L., "Computational Modeling of Turbulent Flows," *Advances in Applied Mechanics*, Vol. 18, 1978, pp. 123–176.

[45]Speziale, C. G., "Analytical Methods for the Development of Reynolds-Stress Closures in Turbulence," *Annual Review of Fluid Mechanics*, Vol. 23, 1991, pp. 107–157.

[46]Craft, T. J., and Launder, B. E., "A Reynolds-Stress Closure Designed for Complex Geometries," *International Journal of Heat and Fluid Flow*, Vol. 17, 1996, pp. 245–254.

[47]Craft, T. J., "Developments in a Low-Reynolds-Number Second-Moment Closure and Its Application to Separating and Reattaching Flows," *International Journal of Heat and Fluid Flow*, Vol. 19, 1998, pp. 541–548.

[48]Shima, N., "Low-Reynolds-Number Second-Moment Closure Without Wall-Reflection Redistribution Terms," *International Journal of Heat and Fluid Flow*, Vol. 19, 1998, pp. 549–555.

[49]Launder, B. E., and Sharma, B. I., "Application of the Energy Dissipation Model of Turbulence to the Calculation of Flows near a Spinning Disk," *Letters in Heat and Mass Transfer*, Vol. 1, 1974, pp. 131–138.

[50]Gerolymos, G. A., and Vallet, I., "Near-Wall Reynolds-Stress Three-Dimensional Transonic Flows Computation," *AIAA Journal*, Vol. 35, No. 2, 1997, pp. 228–236.

[51]Launder, B. E., and Shima, N., "Second-Moment Closure for the Near-Wall Sublayer: Development and Application," *AIAA Journal*, Vol. 27, No. 10, 1989, pp. 1319–1325.

[52]So, R. M. C., Gatski, T. B., and Sommer, T. P., "Morkovin Hypothesis and the Modeling of Wall-Bounded Compressible Turbulent Flows," *AIAA Journal*, Vol. 36, No. 9, 1998, pp. 1583–1592.

[53]Gerolymos, G. A., and Vallet, I., "Implicit Computation of the Three-Dimensional Compressible Navier–Stokes Equations Using k–ε Turbulence Closure," *AIAA Journal*, Vol. 34, No. 7, 1996, pp. 1321–1330.

[54]Durbin, P. A., "On the k–ε Stagnation Point Anomaly," *International Journal of Heat and Fluid Flow*, Vol. 17, 1996, pp. 89, 90.

[55]Schumann, U., "Realizability of Reynolds-Stress Turbulence Models," *Physics of Fluids*, Vol. 20, 1977, pp. 721–725.

[56]Vallet, I., and Gerolymos, G. A., "Near-Wall Reynolds-Stress 3-D Transonic Flows Computations," *2*. ERCOFTAC Workshop on Compressible Turbulence, Oct. 1995.

[57]Craft, T. J., Launder, B. E., and Suga, K., "Prediction of Turbulent Transitional Phenomena with a Nonlinear Eddy-Viscosity Model," *International Journal of Heat and Fluid Flow*, Vol. 18, 1997, pp. 15–28.

[58]Daly, B. J., and Harlow, F. H., "Transport Equations in Turbulence," *Physics of Fluids*, Vol. 13, 1970, pp. 2634–2649.

[59]Hanjalić, K., and Launder, B. E., "A Reynolds Stress Model of Turbulence and Its Application to Thin Shear Flows," *Journal of Fluid Mechanics*, Vol. 52, 1972, pp. 609–638.

[60]Gerolymos, G. A., Sauret, E., and Vallet, I., "Influence of Inflow Turbulence in Shock-Wave/Turbulent-Boundary-Layer Interaction Computations," *AIAA Journal*, Vol. 42, No. 6, 2004, pp. 1101–1106; also AIAA Paper 2003-3465, June 2003.

[61]Reda, D. C., and Murphy, J. D., "Shock-Wave/Turbulent-Boundary-Layer Interactions in Rectangular Channels," *AIAA Journal*, Vol. 11, No. 2, 1973, pp. 139, 140; also AIAA Paper 72-715, 1972.

[62]Murthy, V. S., and Rose, W. C., "Wall Shear Stress Measurements in a Shock-Wave/Boundary-Layer Interaction," *AIAA Journal*, Vol. 16, No. 7, 1978, pp. 667–672.

[63]Modaress, D., and Johnson, D. A., "Investigation of Turbulent Boundary-Layer Separation Using Laser Velocimetry," *AIAA Journal*, Vol. 17, No. 7, 1979, pp. 747–752.

[64]Settles, G. S., Vas, I. E., and Bogdonoff, S. M., "Details of a Shock-Separated Turbulent Boundary-Layer at a Compression Corner," *AIAA Journal*, Vol. 14, No. 12, 1976, pp. 1709–1715.

[65]Horstman, C. C., Settles, G. S., Vas, I. E., T. J., Bogdonoff, S. M., and Hung, C. M., "Reynolds Number Effect on Shock-Wave/Turbulent Boundary-Layer Interactions," *AIAA Journal*, Vol. 15, No. 8, 1977, pp. 1152–1158.

[66]Dolling, D. S., and Murphy, M. T., "Unsteadiness of the Separation Shock-Wave Structure in a Supersonic Compression Ramp Flowfield," *AIAA Journal*, Vol. 21, No. 12, 1983, pp. 1628–1634.

[67]Settles, G. S., and Dodson, L. J., "Supersonic and Hypersonic Shock/Boundary-Layer Interaction Database," *AIAA Journal*, Vol. 32, No. 7, 1994, pp. 1377–1383.

[68]Chassaing, J.-C., Gerolymos, G. A., and Vallet, I., "Turbulence Structure Modification from Shock-Wave Micro-Oscillations," Euromech 440, Sept. 2002.

[69]Reda, D. C., and Murphy, J. D., "Sidewall Boundary-Layer Influence on Shock-Wave/Turbulent-Boundary-Layer Interactions," *AIAA Journal*, Vol. 11, No. 10, 1973, pp. 1367–1368.

R. So
Associate Editor

Color reproductions courtesy of Université Pierre-et-Marie-Curie.